Intracrystalline diffusion regulation of Au/hierarchical TS-1 for simultaneously enhanced stability and selectivity in propene epoxidation with H_2 and O_2

Nan Sheng [a,1], Dong Lin [b,1], Wei Liang [a], Chenyang Zhao [a], Yujia Liu [a], Yunfeng Zhu [a], Zhaoning Song [c], Jie Jiang [a], Wei Xu [a], Zhe Yang [a], Bing Sun [a,*], Xiang Feng [d,*], Chaohe Yang [d]

[a] State Key Laboratory of Chemical Safety, SINOPEC Research Institute of Safety Engineering Co., Ltd., Qingdao 266071, China
[b] Max Planck- Cardiff Centre on the Fundamentals of Heterogeneous Catalysis FUNCAT, Cardiff Catalysis Institute, School of Chemistry, Cardiff University, Cardiff CF24 4HQ, United Kingdom
[c] Department of Chemical Engineering, Tsinghua University, Beijing 100084, China
[d] State Key Laboratory of Heavy Oil Processing, China University of Petroleum, Qingdao 266580, China

A R T I C L E I N F O

Keywords:
Intracrystalline diffusion regulation
Critical micelle concentration
Hierarchical factor
Au/TS-1
Propene epoxidation

A B S T R A C T

Regulation of intracrystalline diffusion plays a pivotal role in ensuring the catalytic stability of metal-supported zeolite catalysts. Herein, we successfully achieved precise modulation of intracrystalline diffusion in Au-loaded hierarchical TS-1 catalysts by two-step recrystallization approach. This modulation was achieved by manipulating the length of mesoporogens, characterized by the hierarchical factor (HF). The HF could be used as the descriptor to reveal the reaction stability and deactivation process including blocking degree (V_{Au}: gold volume / V_{na}: volume not accessible for N_2) by the Au nanoparticles and coke formation in fresh and used catalysts, respectively. In addition, the enhanced selectivity was attributed to the improved hydrophobicity of Au/hierarchical TS-1 with gradually decreased terminal silanols by two-step recrystallization approach. This work not only provides the new strategy for the regulation of zeolite intracrystalline diffusion, but also could shed new lights on the industrial process of direct propene epoxidation with H_2 and O_2.

1. Introduction

Propylene oxide (PO), which is considered as one of the important intermediates in the chemical industry, has widespread applications in automobiles, food, cosmetics, and medicine (Zuwei et al., 2001; Herzberger et al., 2016; McGuire et al., 2016; Lu et al., 2016). PO can be used to synthesize polyether polyol, propylene glycol methyl ether, dimethyl carbonate, and propylene glycol ether (Scho¨mer et al., 2012; Chaniago et al., 2019; Holtbruegge et al., 2013a,b). Among them, polyether polyol is the key raw material for polyurethane synthesis and the main downstream product of propylene oxide (Pokharel, 2014). Moreover, another important downstream product of propylene oxide is dimethyl carbonate, which is considered as the important raw materials of battery electrolyte (Miyoshi et al., 2016; Lee et al., 2020; Barnes et al., 2015). Therefore, the synthesis of PO is attracting more and more attention especially in the gradually emerging fields (e.g., electric automobile, furniture, and coating) (Lin et al., 2020; Feng et al., 2018; Held et al., 2018; Arvay et al., 2022). However, the traditional chlorohydrin method is being phased out because of its serious environmental pollution (Liu et al., 2021; Aly and Saeys, 2021). Therefore, the green direct propene epoxidation with H_2 and O_2 has attracted more and more attention from academic and industrial area due to its environmentally friendly process, easy separation, and high selectivity (Feng et al., 2016; Zhang et al., 2020; Zhang et al., 2021; Wang et al., 2022).

In the direct propene epoxidation with H_2 and O_2, the Au-Ti based catalyst shows superior reaction performance with relatively high propene conversion and PO selectivity compared with other catalysts (e.g., Ag based catalyst, Ni based catalyst, and Ce based catalyst) (Feng et al., 2017; Porter et al., 2021; Teržan et al., 2020). However, the fast deactivation of Au-Ti based catalysts is the key issue in the direct propene epoxidation with H_2 and O2 (Feng et al., 2014; Uphade et al., 2002; Qi et al., 2004; Nijhuis et al., 2005). In order to enhance the catalyst

* Corresponding authors.
E-mail addresses: sunb.qday@sinopec.com (B. Sun), xiangfeng@upc.edu.cn (X. Feng).
[1] These authors contributed equally to this work.

stability, improving the diffusion of propylene oxide to retrain the formation of carbonaceous species in the titanosilicalite channel was considered as the efficient strategy. The channels were pre-blocked to prevent the reactant or product molecules from diffusing into the channels, thus decreasing the content of carbonaceous species in the channel (Feng et al., 2014; Feng et al., 2015). The synthesis of hydrophobic titanosilicalites by silanization and ammonium fluoride treatment to decrease silanol groups (Si-OH) could effectively enhance the desorption of PO molecules, thus restraining the formation of carbonaceous species. In addition, the synthesis of small-sized and mesoporous titanosilicalite could efficiently reduce the diffusion length of PO molecules and further restrain the side reactions of PO molecules (Feng et al., 2017; Song et al., 2020; Sheng et al., 2019). However; these strategies were designed based on the specific titanosilicalite with blocked channels, given particle size or fixed mesoporous diameter, and failed to flexibly regulate the diffusion for reactant and product molecules, thus limiting the application and generality under different conditions.

Herein, the intracrystalline regulation of diffusion in Au/hierarchical TS-1 was achieved based on the controllable carbon chain length of mesoporogens. By increasing the length of carbon chains in the second critical micelle concentration, the pore size of intracrystalline void in the TS-1 support was increased from 4.1 to 19.5 nm. The hierarchical factor (HF) was further proposed to evaluate the intracrystalline diffusion in the TS-1 due to the established positive relationship between the HF and lifetime in propene epoxidation. The HF could be used as the descriptor to reveal the coke formation and blocking degree by the Au nanoparticles (V_{Au}/V_{na}). Moreover, the selectivity could also be improved by the gradually enhanced hydrophobicity of TS-1 with the increase of carbon chain length. This research could offer valuable insights into zeolite synthesis by demonstrating the regulation of intracrystalline diffusion across various reactions, especially in the direct propene epoxidation with simultaneously enhanced stability and selectivity.

2. Experimental section

2.1. *Regulation of pore size in mesoporous titanosilicalite-1 (MTS-1) by two-step recrystallization approach*

The synthesis of crystal seed: 27.9 g of tetrapropylammonium hydroxide (25 wt%, TPAOH, Sinopharm Chemical Reagent Co., Ltd) was added into 6.9 g of deionized water (18.2 MΩ•cm) in a beaker of 250 mL. Then 22.58 g of tetraethyl orthosilicate (TEOS, Sinopharm Chemical Reagent Co., Ltd) was added into the above-mentioned mixture dropwise under stirring for 2 h. Afterwards, 3.6 g of isopropyl alcohol containing 0.184 g of tetrabutyl titanate (TBOT, Sinopharm Chemical Reagent Co., Ltd) was further added into the mixture dropwise under vigorous stirring for 3 h. The mixture with Ti sources, Si sources and template was heated at 80 °C and kept for 3 h to remove alcohol in an open environment without lids. Then the titanosilicalite gel in a Teflon liner of 100 mL was crystallized at 170 °C for 3 days in a static oven. Finally, the crystal seed was centrifuged, washed by water for three times, dried (80 °C) and calcinated at 550 °C (2 °C/min) for 6 h in a furnace with static air to obtain the titanosilicalite seed.

The regulation of pore size: 8.9×10^{-4} mol/L (first critical micelle concentration) or 2.1×10^{-2} mol/L (second critical micelle concentration) of mesoporogen containing octyltrimethylammonium bromide (C8), decyltrimethylammonium bromide (C10), dodecyltrimethylammonium bromide (C12) and cetyltrimethylammonium bromide (C16), 400 ml of ammonia (2.5 wt%) and 4 g of crystal seed were mixed for 3 h. Then, the mixture was recrystallized for 24 h at 140 °C in the Teflon-lined autoclave. Finally, the MTS-1 was obtained by centrifuged, washed, dried (80 °C) and calcinated at 550 °C for 6 h to obtain the MTS-1-CX with specific pore size and the CX represents mesoporogens with different carbon lengths.

2.2. *Synthesis of the Au/MTS-1 catalysts*

The Au/MTS-1 catalysts were prepared by the new modified isometric impregnation (NIMG) method[39]. 0.009 g of chloroauric acid ($HAuCl_4 \cdot 4H_2O$) was mixed with 4.5 g of deionized H_2O. Then 1 mol/L and 0.1 mol/L Na_2CO_3 solutions were added dropwise under vigorous stirring until the pH reached 7.3–7.6. After that, the deionized water was added dropwise until the volume reached 5 ml. Then 0.4 g of solution was added dropwise and impregnated onto the 0.5 g of MTS-1 without stirring. The Au/MTS-1 catalysts were obtained by drying at 30 °C under vacuum (−100 KPa) for 12 h.

2.3. *Characterizations*

The X-ray diffraction (XRD, X′pert PRO MPD) equipped with the Cu Kα radiation was used to confirm the titanosilicalite crystal structure with a scanning speed about 10°/min. The Fourier-transform infrared spectroscopy (FT-IR, Nicolet IS30) was used to determine the framework structure of titanosilicalite pretreated at 80 °C for 8 h in oven, and the reference was KBr powder. The diffuse reflectance Ultraviolet–visible spectroscopy (UV–vis, Shimadzu UV-2700) was used to characterize the Ti species in the titanosilicalite (medium scan speed), and the $BaSO_4$ was used as the background. The nitrogen physical absorption–desorption isotherm was conducted using the Micromeritics ASAP 2460 at 77 K. The various TS-1 powders were pretreated at 573 K for 6 h to eliminate any air and water adsorbed in the channels. Additionally, the different Au/TS-1 catalysts were pretreated at room temperature for 24 h to remove any air and water adsorbed in the channels. The morphology and particle size were observed by the high-resolution transmission electron microscope with an accelerating voltage of 200 kV (HRTEM, JEM-2100UHR). The Au loading and Ti content were measured using inductively coupled plasma optical emission spectrometry (ICP-OES, Agilent 730 ICP-OES). The chemical environment of Si atom in the titanosilicalite framework was characterized by the ^{29}Si solid state magic angle spinning nuclear magnetic resonance (^{29}Si MAS NMR, Bruker 400 M). The thermogravimetry analysis (TG, Netzsch) was used to reveal the coke content of the Au/MTS-1 catalyst (10 °C/min, 30 ~ 1000 °C).

2.4. *Propene epoxidation with H_2 and O_2*

The synthesized Au/MTS-1 catalysts were tested in the fixed bed for the direct propene epoxidation with H_2 and O_2. 0.15 g of Au/MTS-1 catalyst was loaded into a quartz reactor with the outer diameter of 10 mm and inner diameter of 8 mm. The propene reaction was carried out at 200 °C (center of catalyst bed tested by a thermowell) under ambient pressure with a space velocity of 14000 $mL \cdot h^{-1} \cdot g^{-1}_{Cat}$. Moreover, the hydrogen (3.5 mL/min), oxygen (3.5 mL/min), propene (3.5 mL/min), nitrogen (24.5 mL/min) were used as the feed gas. The product was analyzed by the online gas chromatography equipped with the TCD and FID detectors. The propene conversion and propylene oxide selectivity were calculated based on the following equation:

Propene conversion:

$$= \frac{C_3\ moles + (acetaldehyde\ moles \times 2)/3 + (carbon\ dioxide\ moles)/3}{propene\ moles}$$

Propylene epoxide selectivity:

$$= \frac{propylene\ oxide\ moles}{C_3\ moles + (acetaldehyde\ moles \times 2)/3 + (carbon\ dioxide\ moles)/3}$$

3. Results and discussion

3.1. The effect of critical micelle concentration on the hydrothermal synthesis of TS-1

As one of surfactants, cetyltrimethylammonium bromide (CTAB) can form different micelles in the aqueous solutions at different concentra- tions. According to the critical micelle concentration (CMC) theory (Brinker et al., 1999; Brinker, 2013) as shown in the Fig. 1a, the extremely low concentration of CTAB surfactant was dissolved in the aqueous solution in the form of molecules.

As the CTAB concentration increases to the first CMC, the CTAB surfactant self-assembles into a round shape, in which the hydrophilic head points outward and the hydrophilic tail points inward. As the CTAB concentration further increases to the second CMC, the CTAB surfactant self-assembles into a rod-like structure, which is similar to that in the first CMC (Vartuli et al., 1994; Cheng et al., 1995; Vartuli et al., 1994). In order to investigate the effects of different self-assembled structures in the preparation of mesoporous titanosilicalite, precursors with the first and second CMCs were used for in the hydrothermal synthesis.

In the Fig. 1b, The XRD spectra show that both samples (TS-1–1 and TS-1–2) have five typical peaks at 8.0°, 8.8°, 23.1°, 24.0° and 24.5°, which is attributed to the MFI topology structures (Sheng et al., 2022). Moreover, both TS-1–1 and TS-1–2 samples show a single peak at 24.5°, demonstrating the orthorhombic crystal system (Lin et al., 2020). The FT-IR spectra were further used to reveal the titanosilicate framework of TS-1–1 and TS-1–2 samples. The peaks at 550 and 1230 cm^{-1} are considered as the typical characteristics of MFI framework and the peaks at 800 and 1100 cm^{-1} are assigned to the symmetrical and antisym- metrical stretching vibration of tetrahedral framework silicon (SiO_4), respectively (Lv et al., 2019). In addition, the peak at 960 cm^{-1} is identified as the incorporation of Ti atom into the MFI framework (Signorile et al., 2018). The UV–vis spectra were further used to reveal the Ti coordination properties in titanosilicalites. For all samples, the

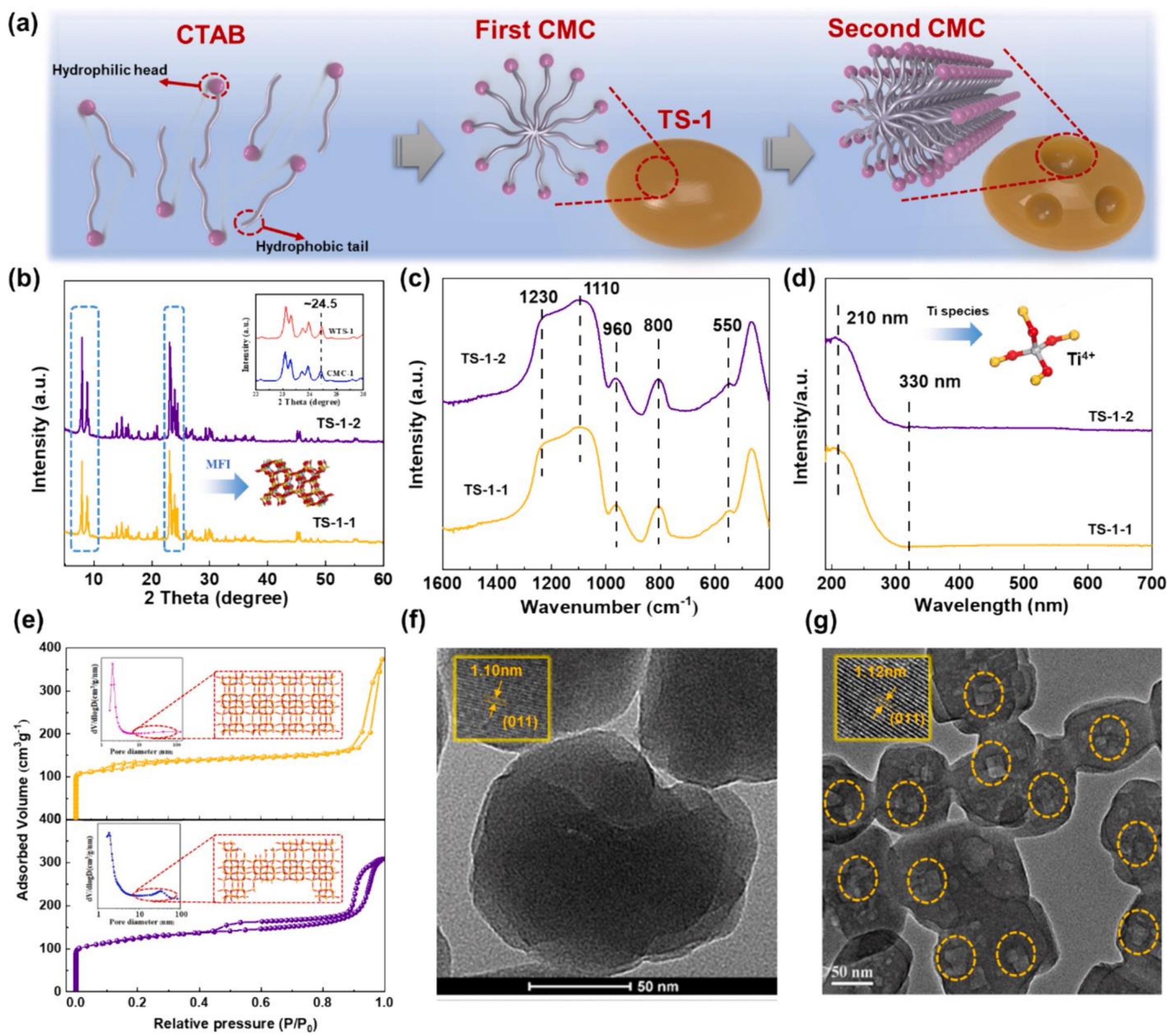

Fig. 1. (a) The schematic diagram of self-assembled structure at different CTAB concentrations. (b) The XRD patterns, (c) FT-IR spectra, (d) UV–vis spectra of different titanosilicalites at first CMC (TS-1–1) and second CMC (TS-1–2). The nitrogen adsorption isotherms of (e) TS-1–1 and TS-1–2 catalysts. The typical HRTEM images of (f) TS-1–1 and (g) TS-1–2 catalysts.

band at 210 nm is attributed to the tetrahedral framework Ti species (TiO_4), consistent with the FT-IR results, and no anatase TiO_2 was observed at 330 nm (Zhang et al., 2018; Yang et al., 2020). These characterizations show that both two different self-assembled structures are favor for the formation of MFI framework type and tetracoordinated framework Ti species.

The pore structure was further investigated in different self-assembled structures of CTAB. In the nitrogen physisorption isotherms (Fig. 1e), the TS-1–1 sample exhibits an isotherm close to Type IV with a hysteresis loop in the relative pressure range of 0.8–1.0. However, the TS-1–2 sample shows a more significant Type-IV isotherm with a typical hysteresis loop in the relative pressure range of 0.4–1.0. The pore size distribution (Fig. 1e) shows that the mesopores of TS-1–1 sample are about 2 nm, while those of TS-1–2 sample are 2 nm and 10–45 nm. Moreover, the typical HRTEM images (Fig. 1f-1 g and S1) also show that the TS-1–2 sample has obvious voids inside its particles compared with the TS-1–1 sample. The lattice space of ca.1.10 nm should be attributed to the (011) plane, which was observed in both two samples (TS-1–1 and TS-1–2), and this plane can be assigned to the peak at 8.0° in the XRD spectra. These findings elucidate that the formation of significant intracrystalline voids within the particles is facilitated by the second critical micelle concentration (CMC), where a rod-like structure emerges. This is in contrast to the first CMC, which results in a circle-like structure and does not contribute to intracrystalline void formation.

3.2. Regulation of hierarchical structure inside titanosilicalite

The hierarchical structure of titanosilicalite was regulated by controlling the carbon chain length of mesoporogens (i.e., C8, C10, C12 and C16) based on the second CMC. In the Fig. 2a, all samples show five similar characteristic peaks (i.e., 8.0°, 8.8°, 23.1°, 24.0° and 24.5°) of MFI framework. Moreover, all samples have a single peak at 24.5°,

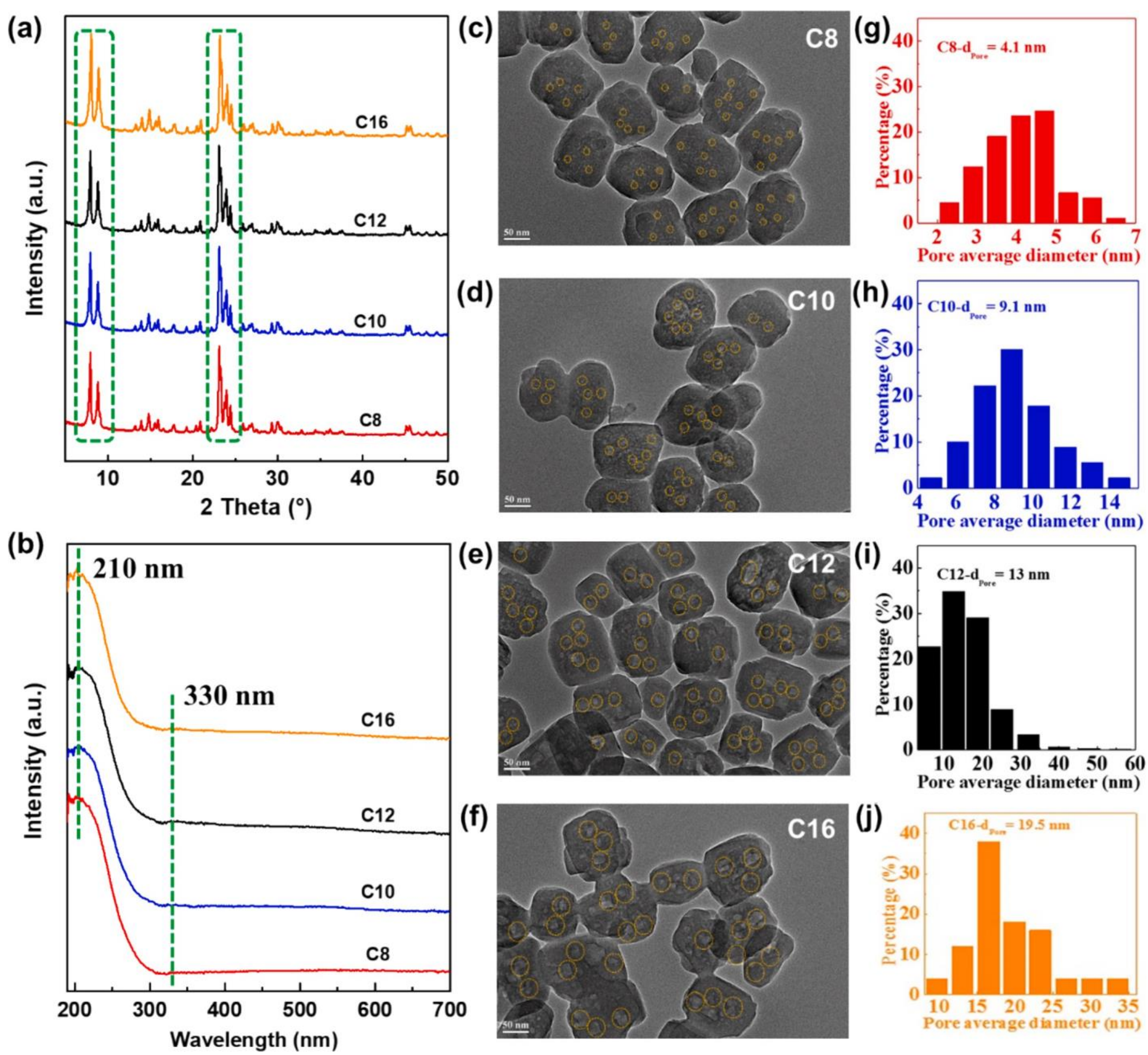

Fig. 2. (a) The XRD patterns and (b) UV–vis spectra of different titanosilicalites synthesized by surfactants with different carbon chains (i.e., C8, C10, C12 and C16). The typical TEM images of titanosilicalites synthesized by (c) C8, (d) C10, (e) C12, and (f) C16 surfactants. The pore average diameter of titanosilicalites synthesized by (g) C8, (h) C10, (i) C12, and (j) C16 surfactants.

which is attributed to the orthorhombic crystal system. The UV–vis spectra were further used to reveal the framework and extra-framework Ti species. In the Fig. 2b, all samples show a single band at 210 nm, which is assigned to the isolated tetrahedral framework Ti species (TiO_4), and no band at 330 nm was found, demonstrating that no anatase TiO_2 exists in the titanosilicalites.

The hierarchical pore structure, which is considered as the key for intracrystalline diffusion in zeolites, was further investigated. The TEM images in Fig. 2c-2f show that all samples are irregularly ellipsoidal particles with the size of about 100 nm. Moreover, it can be clearly seen that the intracrystalline voids gradually become larger with the increase of carbon chain length of mesoporengens. In order to quantitively calculate the average pore size of intracrystalline voids, over 100 voids were counted in each sample. The results are showed in Fig. 2g-2j. It is found that with increasing carbon chain from C8 to C16 by the two-step recrystallization method, the average pore diameter of intracrystalline void increases from 4.1 to 19.5 nm.

The nitrogen adsorption–desorption results were further used to reveal the pore structure (Fig. 3 and Table S1). It is found that with the increase of carbon chain length from C8 to C16 (Fig. 3a), the microporous volume gradually decreased from 0.19 to 0.16 cm^3g^{-1}, while the mesoporous specific surface area gradually increases from 72.3 to 109.5 m^2g^{-1} (Fig. 3b).

In order to quantitatively calculate the hierarchical degree of zeolite, the hierarchical factor (HF) was employed in this manuscript (P´erez-Ramírez et al., 2009; Ivanova and Knyazeva, 2013). The HF is calculated according to the following equation: HF = $(V_{micro}/V_{total}) \times (S_{meso}/S_{BET})$. The parameters V_{micro}/V_{total} and S_{meso}/S_{BET} here represent the proportion of microporous and mesoporous pore structures in the entire pore system, respectively. The product of the two describes the proportion of micropores and mesopores in the overall pore structure of hierarchical zeolite. Different from traditional individual microporous and mesoporous properties, the HF can bridge the relationship between the micropores and mesopores in the zeolite. From the Fig. 3c, it can be seen that with the increase of carbon chain length from C8 to C16, the HF gradually increased from 0.056 to 0.084. The highest HF (0.084) of MTS-1-C16 titanosilicalite demonstrates that the mesopores are maximized without the severe penalization of micropores. In addition, it is found that there is a linear relationship between HF and the length of carbon chain of surfactants, as shown in the Fig. 3d. The positive linear equation is $y = 3.36 \times 10^{-3}x + 0.032$ (x: length of carbon chain, y: HF). Therefore, based on the two-step recrystallization method, the hierarchical structure described by the HF can be regulated by adjusting the carbon chain length.

3.3. *Improving the catalytic performance by regulation of intracrystalline diffusion*

The titanosilicalites with regulated mesoporous structure were loaded with Au nanoparticles and further tested in the propene epoxidation with H_2 and O_2. The Fig. 4a shows that in the presence of the different catalysts, the PO formation rate is a function of time on stream. It is found that the Au/MTS-1-C8, Au/MTS-1-C10 and Au/MTS-1-C12 catalysts start to significantly deactivate after propene epoxidation for 6, 13 and 17 h, respectively. This deactivation is attributed to the blocking of micropores by carbonaceous deposits. The Au deposited on the external surface remains active for propene epoxidation, which leads to the initial deactivation and ensures continued stable propene epoxidation. However, the Au/MTS-1-C16 catalysts keep stable during the initial 25 h. It was found that there is a positive relationship between the HF of different titanosilicalite supports and their lifetimes in propene epoxidation. The progressively enhanced catalytic stability can be attributed to the improved diffusion properties, as indicated by the HF values in the different titanosilicates.

In addition, the slightly decreased initial PO formation rate of Au/MTS-1-C16 catalyst should be attributed to fewer Au nanoparticles into the micropores. The micropores can boost the formation of small- sized Au nanoparticles with more corner active sites, thus enhancing

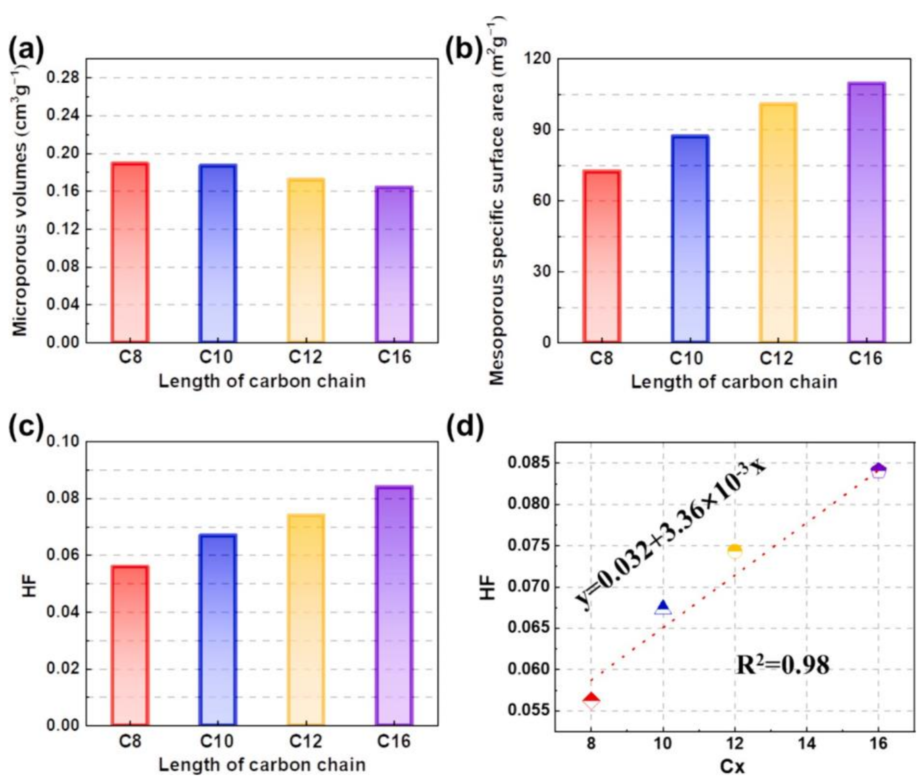

Fig. 3. (a) The microporous volumes, (b) mesoporous specific surface area and (c) HF of titanosilicalites synthesized by surfactants with different carbon chains (i.e., C8, C10, C12 and C16), (d) the linear relationship between the HF of different titanosilicalites and length of carbon chains.

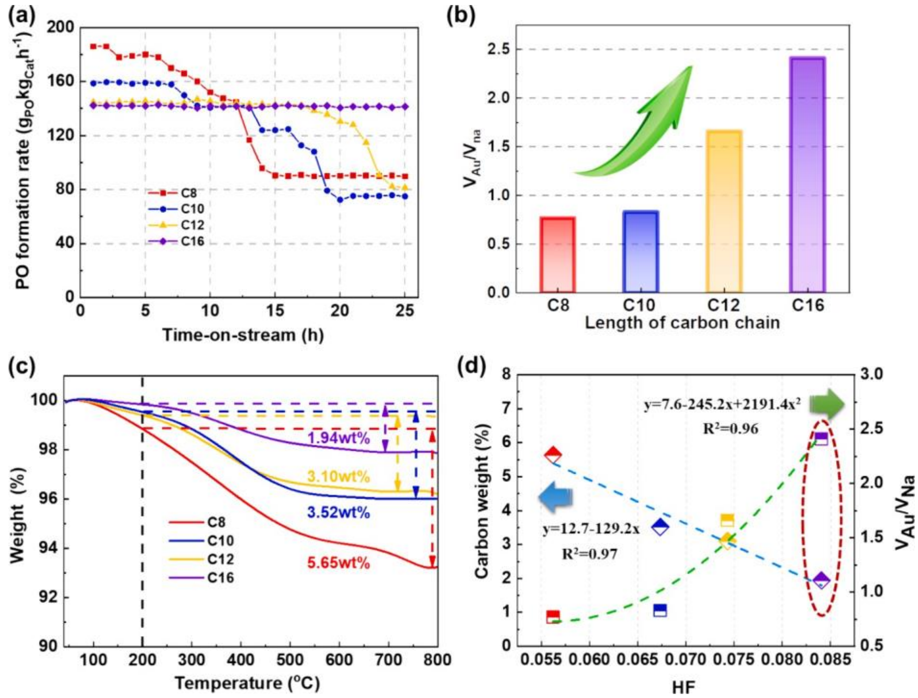

Fig. 4. (a) The PO formation rate with different catalysts at time-on stream, (b) the V_{Au}/V_{na} and (c) TG profiles of different catalysts after propene epoxidation with H_2 and O_2 for 25 h, (d) the relationship between the HF, carbon content and V_{Au}/V_{na}.

the initial PO formation rate (Feng et al., 2018; Li et al., 2017; Lee et al., 2012). Table S2 shows that the increase of carbon chain length from C8 to C16, the difference between the microporous volumes before and after Au loading gradually decreases from 40.2 to 5.5 %, further demonstrating that with the increase of HF value, more Au nanoparticles are not located in the micropores but in the mesopores. Although the initial PO formation rate slightly decreases with increasing HF of titanosilicalite supports, the catalytic stability of propene epoxidation is significantly enhanced by the regulated diffusion in the titanosilicalite supports. Therefore, the mesopores should be maximized without severe penalization of micropores. This is in accordance with the definition of HF which bridges the relationship between the micropores and mesopores.

Moreover, the descriptor (V_{Au}/V_{na}) can be used to estimate the degree of zeolite channel blockage by the Au nanoparticles shown in the Fig. 4b. Among them, the V_{Au} and V_{na} represent the volume of gold and the volume which is not accessible for probe molecules (N_2), respectively. The progressively rising V_{Au}/V_{na} ratio indicates that titanosilicates with higher HF values can efficiently mitigate blockages caused by the Au nanoparticles, thereby improving the positioning of the Au nanoparticles.

In the direct propene epoxidation with Au-Ti based catalyst, the channel blockage by the Au nanoparticles and carbonaceous species is major reason for catalyst deactivation. The formation of carbonaceous species could be evaluated by the thermogravimetric analysis (TGA) shown in the Fig. 4c. The TGA profiles demonstrated that the improved diffusion with the increase of HF can effectively decrease the formation of carbonaceous species in the Au/MTS-1 catalysts. The Au/MTS-1-C16 catalyst has the lowest carbon deposition (1.94 wt%) compared with those on the Au/MTS-1-C8 (5.65 wt%), Au/MTS-1-C10 (3.52 wt%) and Au/MTS-1-C12 (3.10 wt%) catalysts after the propene epoxidation for 25 h. The relationship between the carbon deposition and HF can be established as follows: $y = 12.7–129.2x$ (y: carbon content, x: HF). Hence, the intracrystalline diffusion, as characterized by the HF in the Au/MTS-1 catalysts, can be systematically controlled to manage carbon deposition. This control is achieved through the manipulation of carbon chain length using the two-step recrystallization method.

In the Fig. 4d, it is found that there is a negative linear relationship between the HF of different titanosilicalite supports and carbon content in the propene epoxidation, and the equation is $y = 12.7–129.2x$. Moreover, there is a positive relationship between the HF and V_{Au}/V_{na} ($y = 7.6–245.2x + 2191.4x^2$). Therefore, a higher HF can effectively inhibit the formation of coke and prevent blockage by Au nanoparticles, thereby enhancing diffusion during propene epoxidation with H_2 and O_2. Based on the established relationship, HF can serve as an indicator for the degree of channel blockage caused by coke and Au nanoparticles.

The PO selectivity of different catalysts as a function of time on stream during the catalytic period of 25 h was further showed in the Fig. 5a. It is found that with the increase of length of carbon chain, the PO selectivity gradually increases from 60 to 90 %. The Au/MTS-1-C16 catalyst not only shows the highest PO selectivity (~90 %) but also the best stability (~25 h) than Au/MTS-1-C8, Au/MTS-1-C10 and Au/MTS-1-C12 catalysts. The gradually enhanced selectivity should be attributed to the enhanced diffusion of PO with higher HF and improved hydrophobicity of titanosilicalite supports. The higher HF and more hydrophobicity could restrain the ring-opening reaction of PO and formation for aromatic carbonaceous deposits, thus improving the catalytic selectivity.

In Fig. 5d-5 g, the peaks at −104 and −113 ppm should be assigned to the $(SiO)_3SiOH$ (Q_3) and $(SiO)_4Si$ (Q_4) species, respectively (Lin et al., 2021). The signal at −116 ppm should be attributed to the orthorhombic symmetry of MFI titanosilicalites (Wu et al., 2014). A decrease in surface hydroxyl groups (resulting in a lower Q_3/Q_4 value) indicates increased hydrophobicity, which is beneficial for the desorption of propylene oxide (PO) and the suppression of side reactions on the catalyst surface. Therefore, the ratio of Q_3/Q_4 was used to determine the hydrophobicity of zeolite supports (Na et al., 2011; Song et al., 2019). It can be seen from Fig. 5d-5 g that with the increase of length of carbon chain, the value of Q_3/Q_4 gradually decreases from 14.68 to 8.92 %. The higher hydro- phobicity of zeolite supports with higher HF should be attributed to the lower specific surface area (Fig. 5b). The lower specific surface area can restrain the formation of terminal silanol species as shown in the Fig. 5h. It demonstrates that the higher HF can effectively enhance the hydrophobicity of MTS-1 supports, thus boosting the desorption of PO and

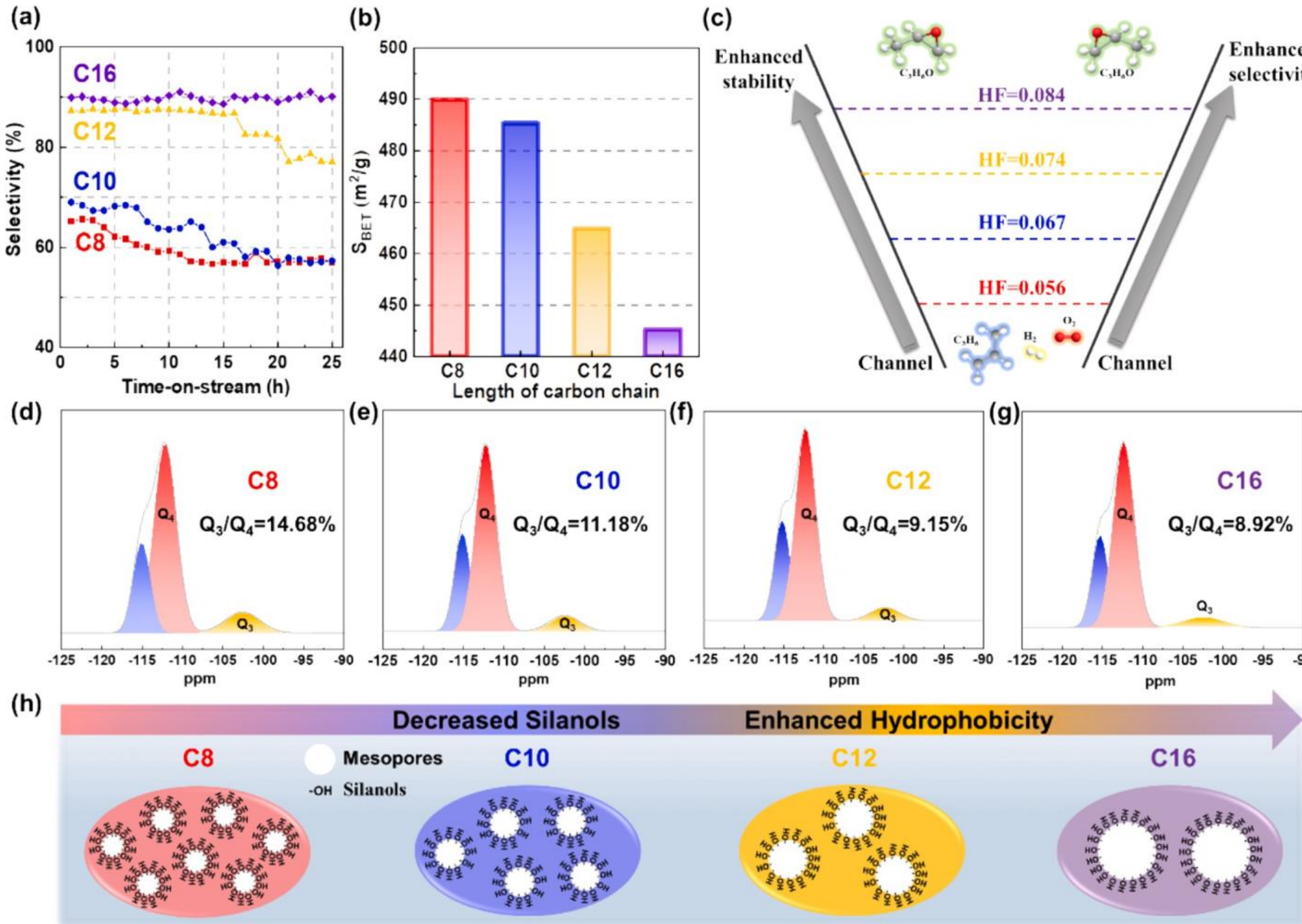

Fig. 5. (a) The PO selectivity with different catalysts at time-on stream, (b) the BET surface area of different titanosilicalites, (c) the schematic diagram of the relationship between the regulated diffusion described by the HF and the reaction performance, the ^{29}Si MAS NMR spectra of (d) MTS-1-C8 (e) MTS-1-C10 (f) MTS-1-C12 (g) MTS-1-C16 supports, and (h) the schematic diagram of the silanols in the different titanosilicalites.

further providing higher selectivity. Therefore, the regulation of HF as a descriptor of diffusion and further improved hydrophobicity of zeolite supports could simultaneously effectively enhance the catalytic stability and selectivity of propene epoxidation with H_2 and O_2 by enhancing the diffusion in the channel of titanosilicalite supports and the desorption of propene oxide (Fig. 5c).

4. Conclusion

In summary, the regulation of intracrystalline diffusion in the Au/hierarchical TS-1 were prosed to simultaneously enhance the stability and selectivity of propene epoxidation with H_2 and O_2 based on the critical micelle concentration (CMC) theory. The second CMC with a rod-like structure could boost the formation of intracrystalline voids inside particle compared with the first CMC. Based on the second CMC, the hierarchy factor (HF) which bridges the relationship between the mesopores and micropores was proposed to describe the intracrystalline diffusion due to the established positive relationship between the HF and lifetime as follows: y = 674.1x-32.3 (x: HF, y: lifetime), and it can be regulated by changing the carbon chain length from C8 to C16. With the gradual increase of HF from 0.056 to 0.084 (size of intracrystalline voids from 4.1 to 19.5 nm), the stability of propene epoxidation was enhanced from 6 to 25 h due to the enhanced intracrystalline diffusion. The HF could be used as the descriptor to reveal the coke formation (y = 12.7–129.2x) and blocking degree (V_{Au}/V_{na}) by the Au nanoparticles (y = 7.6–245.2x + 2191.4x^2). Moreover, the selectivity of propylene oxide was simultaneously increased from 60 to 90 %, which is attributed to the enhancement of hydrophobicity with the decrease of terminal silanols by two-step recrystallization approach. This work not only provides the new method for regulating the diffusion of zeolites, but also paves the way for the industrial production of propene epoxidation with H_2 and O_2.

CRediT authorship contribution statement

Nan Sheng: Writing – original draft, Visualization, Validation, Formal analysis, Conceptualization. **Dong Lin:** Writing – original draft, Visualization, Validation, Formal analysis, Conceptualization. **Wei Liang:** Writing – review & editing, Conceptualization. **Chenyang Zhao:** Writing – review & editing. **Yujia Liu:** Writing – review & editing. **Yunfeng Zhu:** Writing – review & editing. **Zhaoning Song:** Writing – review & editing, Conceptualization. **Jie Jiang:** Writing – review & editing, Conceptualization. **Wei Xu:** Writing – review & editing, Conceptualization. **Zhe Yang:** Writing – review & editing, Conceptualization. **Bing Sun:** Writing – review & editing, Supervision, Resources, Project administration. **Xiang Feng:** Writing – review & editing, Supervision, Resources, Project administration. **Chaohe Yang:** Supervision, Resources, Project administration.

Declaration of competing interest

The authors declare that they have no known competing financial interests or personal relationships that could have appeared to influence the work reported in this paper.

Data availability

Data will be made available on request.

Acknowledgements

This work was supported by the National Natural Science Foundation of China (21978325), the Natural Science Foundation of Shandong Province (ZR2020KB006) and the Outstanding Youth Fund of Shandong Provincial Natural Science Foundation (ZR2020YQ17).

Appendix A. Supplementary data

Supplementary data to this article can be found online at https://doi.org/10.1016/j.ces.2024.120538.

References

Aly, M., Saeys, M., 2021. Selective silylation boosts propylene epoxidation with H_2 and O_2 over Au/TS-1. Chem Catal. 1, 761–762.

Arvay, J.W., Hong, W., Li, C., Delgass, W.N., Ribeiro, F.H., Harris, J.W., 2022. Kinetics of propylene epoxidation over extracrystalline gold active sites on AU/TS-1 catalysts. ACS Catal. 12, 10147–10160.

Barnes, T.A., Kaminski, J.W., Borodin, O., Miller III, T.F., 2015. Ab initio characterization of the electrochemical stability and solvation properties of condensed-phase ethylene carbonate and dimethyl carbonate mixtures. J. Phys. Chem. C 119, 3865–3880.

Brinker, C.J., 2013. Dip coating. In: Chemical Solution Deposition of Functional Oxide Thin Films. Springer, pp. 233–261.

Brinker, C.J., Lu, Y., Sellinger, A., Fan, H., 1999. Evaporation-induced self-assembly: nanostructures made easy. Adv. Mater. 11, 579–585.

Chaniago, Y.D., Hussain, A., Andika, R., Lee, M., 2019. Reactive pressure-swing distillation toward sustainable process of novel continuous ultra-high-purity electronic-grade propylene glycol monomethyl ether acetate manufacture. ACS Sustain. Chem. Eng. 7, 18677–18689.

Cheng, C.-F., Luan, Z., Klinowski, J., 1995. The role of surfactant micelles in the synthesis of the mesoporous molecular sieve MCM-41. Langmuir 11, 2815–2819.

Feng, X., Duan, X., Qian, G., Zhou, X., Chen, D., Yuan, W., 2014. Au nanoparticles deposited on the external surfaces of TS-1: Enhanced stability and activity for direct propylene epoxidation with H_2 and O_2. Appl. Catal. B: Environ. 150, 396–401.

Feng, X., Duan, X., Qian, G., Zhou, X., Chen, D., Yuan, W., 2014. Insights into size-dependent activity and active sites of Au nanoparticles supported on TS-1 for propene epoxidation with H_2 and O_2. J. Catal. 317, 99–104.

Feng, X., Duan, X., Yang, J., Qian, G., Zhou, X., Chen, D., Yuan, W., 2015. Au/uncalcined TS-1 catalysts for direct propene epoxidation with H_2 and O_2: effects of Si/Ti molar ratio and Au loading. Chem. Eng. J. 278, 234–239.

Feng, X., Liu, Y., Li, Y., Yang, C., Zhang, Z., Duan, X., Zhou, X., Chen, D., 2016. Au/TS-1 catalyst for propene epoxidation with H_2/O_2: a novel strategy to enhance stability by tuning charging sequence. AlChE J. 62, 3963–3972.

Feng, X., Sheng, N., Liu, Y., Chen, X., Chen, D., Yang, C., Zhou, X., 2017. Simultaneously enhanced stability and selectivity for propene epoxidation with H_2 and O_2 on Au catalysts supported on nano-crystalline mesoporous TS-1. ACS Catal. 7, 2668–2675.

Feng, X., Song, Z., Liu, Y., Chen, X., Jin, X., Yan, W., Yang, C., Luo, J., Zhou, X., Chen, D., 2018. Manipulating gold spatial location on titanium silicalite-1 to enhance the catalytic performance for direct propene epoxidation with H_2 and O_2. ACS Catal. 8, 10649–10657.

Feng, X., Yang, J., Duan, X., Cao, Y., Chen, B., Chen, W., Lin, D., Qian, G., Chen, D., Yang, C., 2018. Enhanced catalytic performance for propene epoxidation with H_2 and O_2 over bimetallic Au–Ag/uncalcined titanium silicate-1 catalysts. ACS Catal. 8, 7799–7808.

Held, A., Kowalska-Ku´s, J., Millot, Y., Averseng, F., Calers, C., Valentin, L., Dzwigaj, S., 2018. Influence of the preparation procedure of vanadium-containing SiBEA zeolites on their catalytic activity in propene epoxidation. J. Phys. Chem. C 122, 18570–18582.

Herzberger, J., Niederer, K., Pohlit, H., Seiwert, J., Worm, M., Wurm, F.R., Frey, H., 2016. Polymerization of ethylene oxide, propylene oxide, and other alkylene oxides: synthesis, novel polymer architectures, and bioconjugation. Chem. Rev. 116, 2170–2243.

Holtbruegge, J., Leimbrink, M., Lutze, P., Go´rak, A., 2013a. Synthesis of dimethyl carbonate and propylene glycol by transesterification of propylene carbonate with methanol: Catalyst screening, chemical equilibrium and reaction kinetics. Chem. Eng. Sci. 104, 347–360.

Holtbruegge, J., Heile, S., Lutze, P., Go´rak, A., 2013b. Synthesis of dimethyl carbonate and propylene glycol in a pilot-scale reactive distillation column: experimental investigation, modeling and process analysis. Chem. Eng. J. 234, 448–463.

Ivanova, I.I., Knyazeva, E.E., 2013. Micro–mesoporous materials obtained by zeolite recrystallization: synthesis, characterization and catalytic applications. Chem. Soc. Rev. 42, 3671–3688.

Lee, H., Hwang, S., Kim, M., Kwak, K., Lee, J., Han, Y.-K., Lee, H., 2020. Why does dimethyl carbonate dissociate Li salt better than other linear carbonates? Critical role of polar conformers. J. Phys. Chem. Lett. 11, 10382–10387.

Lee, W.-S., Lai, L.-C., Akatay, M.C., Stach, E.A., Ribeiro, F.H., Delgass, W.N., 2012. Probing the gold active sites in Au/TS-1 for gas-phase epoxidation of propylene in the presence of hydrogen and oxygen. J. Catal. 296, 31–42.

Li, Z., Zhang, J., Wang, D., Ma, W., Zhong, Q., 2017. Confirmation of gold active sites on titanium-silicalite-1-supported nano-gold catalysts for gas-phase epoxidation of propylene. J. Phys. Chem. C 121, 25215–25222.

Lin, D., Zheng, X., Feng, X., Sheng, N., Song, Z., Liu, Y., Chen, X., Cai, Z., Chen, D., Yang, C., 2020. Enhancing the dynamic electron transfer of Au species on wormhole-like TS-1 for boosting propene epoxidation performance with H_2 and O_2. Green Energy Environ. 5, 433–443.

Lin, D., Zhang, Q., Qin, Z., Li, Q., Feng, X., Song, Z., Cai, Z., Liu, Y., Chen, X., Chen, D., 2021. Reversing titanium oligomer formation towards high-efficiency and green synthesis of titanium-containing molecular sieves. Angew. Chem. Int. Ed. 60, 3443–3448.

Liu, Y., Zhao, C., Sun, B., Zhu, H., Xu, W., 2021. Preparation and modification of Au/TS-1 catalyst in the direct epoxidation of propylene with H_2 and O_2. Appl. Catal. a: Gen. 624, 118329.

Lu, X., Wu, H., Jiang, J., He, M., Wu, P., 2016. Selective synthesis of propylene oxide through liquid-phase epoxidation of propylene with H_2O_2 over formed Ti-MWW catalyst. J. Catal. 342, 173–183.

Lv, G., Deng, S., Yi, Z., Zhang, X., Wang, F., Li, H., Zhu, Y., 2019. One-pot synthesis of framework W-doped TS-1 zeolite with robust Lewis acidity for effective oxidative desulfurization. Chem. Commun. 55, 4885–4888.

McGuire, B.A., Carroll, P.B., Loomis, R.A., Finneran, I.A., Jewell, P.R., Remijan, A.J., Blake, G.A., 2016. Discovery of the interstellar chiral molecule propylene oxide (CH3CHCH2O). Science 352, 1449–1452.

Miyoshi, S., Nagano, H., Fukuda, T., Kurihara, T., Watanabe, M., Ida, S., Ishihara, T., 2016. Dual-carbon battery using high concentration $LiPF_6$ in dimethyl carbonate (DMC) electrolyte. J. Electrochem. Soc. 163, A1206.

Na, K., Jo, C., Kim, J., Ahn, W.-S., Ryoo, R., 2011. MFI titanosilicate nanosheets with single-unit-cell thickness as an oxidation catalyst using peroxides. ACS Catal. 1, 901–907.

Nijhuis, T.A., Gardner, T.Q., Weckhuysen, B.M., 2005. Modeling of kinetics and deactivation in the direct epoxidation of propene over gold–titania catalysts. J. Catal. 236, 153–163.

P´erez-Ramírez, J., Verboekend, D., Bonilla, A., Abello´, S., 2009. Zeolite catalysts with tunable hierarchy factor by pore-growth moderators. Adv. Funct. Mater. 19, 3972–3979.

Pokharel, P., 2014. High performance polyurethane nanocomposite films prepared from a masterbatch of graphene oxide in polyether polyol. Chem. Eng. J. 253, 356–365.

Porter, W.N., Lin, Z., Chen, J.G., 2021. Experimental and theoretical studies of reaction pathways of direct propylene epoxidation on model catalyst surfaces. Surf. Sci. Rep. 76, 100524.

Qi, C., Okumura, M., Akita, T., Haruta, M., 2004. Vapor-phase epoxidation of propylene using H_2/O_2 mixture over gold catalysts supported on non-porous and mesoporous titania-silica: Effect of preparation conditions and pretreatments prior to reaction. Appl. Catal. a: Gen. 263, 19–26.

Scho¨mer, M., Seiwert, J., Frey, H., 2012. Hyperbranched poly (propylene oxide): a multifunctional backbone-thermoresponsive polyether polyol copolymer. ACS Macro Letters 1, 888–891.

Sheng, N., Liu, Z., Song, Z., Lin, D., Feng, X., Liu, Y., Chen, X., Chen, D., Zhou, X., Yang, C., 2019. Enhanced stability for propene epoxidation with H_2 and O_2 over wormhole-like hierarchical TS-1 supported Au nanocatalyst. Chem. Eng. J. 377, 119954.

Sheng, N., Song, Z., Yuan, J., Liang, W., Zhao, J., Zhang, J., Xu, W., Sun, B., Feng, X., Yang, Z., 2022. Effective regulation of the Au spatial position in a hierarchically structured Au/HTS-1 catalyst: to boost the catalytic performance of propene epoxidation with H_2 and O_2. ACS Sustain. Chem. Eng. 10, 9515–9524.

Signorile, M., Crocella`, V., Damin, A., Rossi, B., Lamberti, C., Bonino, F., Bordiga, S., 2018. Effect of Ti speciation on catalytic performance of TS-1 in the hydrogen peroxide to propylene oxide reaction. The Journal of Physical Chemistry C 122, 9021–9034.

Song, Z., Feng, X., Sheng, N., Lin, D., Li, Y., Liu, Y., Chen, X., Chen, D., Zhou, X., Yang, C., 2019. Cost-efficient core-shell TS-1/silicalite-1 supported Au catalysts: towards enhanced stability for propene epoxidation with H_2 and O_2. Chem. Eng. J. 377, 119927.

Song, Z., Feng, X., Sheng, N., Lin, D., Li, Y., Liu, Y., Chen, X., Zhou, X., Chen, D., Yang, C., 2020. Propene epoxidation with H_2 and O_2 on Au/TS-1 catalyst: cost-effective synthesis of small-sized mesoporous TS-1 and its unique performance. Catal. Today 347, 102–109.

Terzan, J., Hus, M., Likozar, B., Djinović, P., 2020. Propylene epoxidation using molecular oxygen over copper-and silver-based catalysts: a review. ACS Catal. 10, 13415–13436.

Uphade, B., Akita, T., Nakamura, T., Haruta, M., 2002. Vapor-phase epoxidation of propene using H_2 and O_2 over Au/Ti–MCM-48. J. Catal. 209, 331–340.

Vartuli, J., Schmitt, K., Kresge, C., Roth, W., Leonowicz, M., McCullen, S., Hellring, S., Beck, J., Schlenker, J., 1994. Effect of surfactant/silica molar ratios on the formation of mesoporous molecular sieves: inorganic mimicry of surfactant liquid-crystal phases and mechanistic implications. Chem. Mater. 6, 2317–2326.

Vartuli, J., Kresge, C., Leonowicz, M., Chu, A., McCullen, S., Johnson, I., Sheppard, E., 1994. Synthesis of mesoporous materials: liquid-crystal templating versus intercalation of layered silicates. Chem. Mater. 6, 2070–2077.
Wang, G., Du, W., Zhang, Z., Tang, Y., Xu, J., Cao, Y., Qian, G., Duan, X., Yuan, W., Zhou, X., 2022. Combining trace Pt with surface silylation to boost Au/uncalcined TS-1 catalyzed propylene epoxidation with H_2 and O_2. AlChE J. 68, e17416.
Wu, Z., Goel, S., Choi, M., Iglesia, E., 2014. Hydrothermal synthesis of LTA-encapsulated metal clusters and consequences for catalyst stability, reactivity, and selectivity. J. Catal. 311, 458–468.
Yang, G., Han, J., Qiu, Z., Chen, X., Feng, Z., Yu, J., 2020. An amino acid-assisted approach to fabricate nanosized hierarchical TS-1 zeolites for efficient oxidative desulfurization. Inorg. Chem. Front. 7, 1975–1980.
Zhang, T., Chen, X., Chen, G., Chen, M., Bai, R., Jia, M., Yu, J., 2018. Synthesis of anatase-free nano-sized hierarchical TS-1 zeolites and their excellent catalytic performance in alkene epoxidation. J. Mater. Chem. A 6, 9473–9479.
Zhang, Z., Zhao, X., Wang, G., Xu, J., Lu, M., Tang, Y., Fu, W., Duan, X., Qian, G., Chen, D., 2020. Uncalcined TS-2 immobilized Au nanoparticles as a bifunctional catalyst to boost direct propylene epoxidation with H_2 and O_2. AlChE J. 66, e16815.
Zhang, M., Zuo, Y., Li, T., Liu, M., Yang, H., Guo, X., 2021. Kinetics simulation of propylene epoxidation over different Ti species in TS-1. AlChE J. 67, e17261.
Zuwei, X., Ning, Z., Yu, S., Kunlan, L., 2001. Reaction-controlled phase-transfer catalysis for propylene epoxidation to propylene oxide. Science 292, 1139–1141.